Optical Materials 47 (2015) 310–314

Contents lists available at ScienceDirect

Optical Materials

journal homepage: www.elsevier.com/locate/optmat

Femtosecond laser fabrication of waveguides in Rhodamine B-doped GPTS/TEOS-derived organic/silica monolithic xerogel

P.H.D. Ferreira [a,*], A.J.G. Otuka [b], E.C. Barbano [b], D.S. Manoel [c], F.S. De Vicente [c], D.R. Vollet [c], D.A. Donatti [c], L. Misoguti [b], C.R. Mendonça [b]

[a] Departamento de Física, Universidade Federal de São Carlos, 13565-905 São Carlos, SP, Brazil
[b] Instituto de Física de São Carlos, Universidade de São Paulo, 13560-970 São Carlos, SP, Brazil
[c] Departamento de Física, Universidade Estadual Paulista UNESP, Av. 24A 1515, Rio Claro, SP 13506-900, Brazil

ARTICLE INFO

Article history:
Received 29 January 2015
Received in revised form 25 May 2015
Accepted 26 May 2015
Available online 3 June 2015

Keywords:
Organic/silica monolithic xerogels
Femtosecond laser micromachining
Rhodamine B
Waveguides

ABSTRACT

This paper reports on the fabrication and characterization of waveguides inside of a dye doped-organic/inorganic bulk material using femtosecond laser microfabrication. Rhodamine B-doped GPTS/TEOS-derived organic/silica monolithic xerogels with excellent optical quality were prepared by sol–gel method. The influence of the dye concentration on the samples optical properties was also investigated in order to choose the proper one to be used for producing the waveguides. After investigation of parameters to fabrication in xerogels, such as, scan speed effects and pulse energy, we produced waveguides in bulks doped with 0.5 mmol/L of Rhodamine B. Propagation losses in the single mode waveguides, at 632.8 nm wavelength, were obtained.

1. Introduction

In the last few years, there has been a growth attention on methods to process materials for the development of devices. Femtosecond laser (fs-laser) micromachining has prompted as a potential approach in this direction, enabling the production of several optical devices, from interferometers and gratings to waveguide couplers, switches and amplifiers [1–8]. This technique presents several advantages when compared to other approaches, such as photolithography, high-energy ion implantation and reactive ion etching [9]. The latter methods often need prior design and fabrication of masks, require several processing steps and are inherently planar technologies, while fs-laser micromachining allows single-step, maskless and direct processing [9–12]. Furthermore, micromachining with fs-laser pulses also allows the production of 3D micro- and nano-structures, such as super-hydrofobic surfaces, doped-microstructures and nanogratings [13–15].

The interest on the development of organic/inorganic hybrid materials via sol–gel process aiming applications in optics has attracted significant attention because it is possible to obtain silica-based dense bulks at temperatures of synthesis near room temperature with possibility of doping these materials with organic and/or inorganic components. Furthermore, sol–gel derived materials can combine the advantages of inorganic components with those of organic polymers, obtaining materials with enhanced optical quality, significant chemistry stability, considerable mechanical and other properties associated with the interaction of the individual organic and inorganic constituents [16–18]. Owing to the combination of the optical functionality of the organic dye with the high stability of the organic/inorganic matrices, these materials have been recognized as promising candidates in many areas, such as microelectronics and optics [19,20], finding important applications in optical physics, such as new laser materials [21].

The sol–gel technique has been largely explored to obtain organic/silica hybrid materials [18,19,22]. A typical trialkoxysilane precursor used in sol–gel processes is the 3-Glycidoxypropyltrim ethoxysilane (GPTS). This compound possesses functionality of both, silicon alkoxide and the terminal epoxy group [23], and it has been applied in different areas, such as biomaterials, membranes, corrosion- and scratch-resistant coatings for optical applications [22,24,25]. Tetraethyl orthosilicate (TEOS) can be easily converted into silicon dioxide through hydrolysis and polycondensation at room temperature, allowing obtaining a range of structures, such as monodisperse silica particles or polymeric silica networks, depending on the conditions of the synthesis [26]. GPTS/TEOS-derived organic/silica hybrids are of wide interest because the resulting material exhibits specific characteristics of

* Corresponding author.
E-mail address: paulohdf@ufscar.br (P.H.D. Ferreira).

http://dx.doi.org/10.1016/j.optmat.2015.05.047
0925-3467/

each alkoxysilane precursors, as well as their own characteristics which can be controlled by changing sol–gel processing parameters. Furthermore, organic chromophores can be used to dope GPTS/TEOS-derived hybrid materials, to produce new materials with important applications in photonics, such as solid-state dye lasers [27].

Rhodamine B-doped silica/polymer-based matrices have been studied for applications as organic light emitting diodes (OLEDs) [28] and as biosensors [29,30]. In recent work we showed that luminescent quantum dots embedded in GPTS/TEOS-derived organic/silica matrix presented increased emission quantum efficiency [31]. Also, recent results from our group showed that GPTS/TEOS-derived organic/silica hybrids doped with Rhodamine B are potential candidates for random laser applications.

Among several chromophores used for doping, Rhodamine B [32,33] has received great attention due to its high quantum efficiency and singular laser properties. Combining the properties of the organic/inorganic hybrid matrices with the optical functionality of the organic dye, these materials have been recognized as promising candidates for the next-generation of integrated devices.

In this work, we demonstrate the waveguides fabrication by femtosecond laser micromachining inside the bulk of GPTS/TEOS-derived organic/silica monolithic xerogels doped with Rhodamine B for the first time. We initially studied the optimal Rhodamine B concentration that can be incorporated in the GPTS/TEOS-derived organic/silica sols, regarding its intensity of fluorescence in function of different dye concentrations.

After investigating the experimental conditions for waveguides fabrication in the Rhodamine B-doped GPTS/TEOS-derived samples, they were characterized by optical microscopy, revealing interesting details of its morphology. We demonstrated the functionality of the fabricated waveguides by measuring the near-field intensity distribution at the waveguide output, as well as its guiding efficiency. Finally, by using the Z-scan technique [34], the self-focusing effect in the central region of the fabricated waveguide was analyzed.

2. Experimental setup

The Rhodamine B-doped GPTS/TEOS-derived samples were prepared by sol–gel technique. Sols of GPTS/TEOS-derived organic/Silica hybrids were prepared by acid hydrolysis of 3-Glyc idoxypropyltrimethoxysilane (GPTS) (Aldrich 98%) and Tetraethyl orthosilicate (TEOS) (Aldrich 99%) silicon alkoxides mixture dissolved in ethanol (EtOH). A 0.6 M solution of HNO_3 in water was slowly dropped into the alkoxides mixtures for acid catalyzed hydrolysis. The nominal GPTS/TEOS/EtOH/H_2O/HNO_3 molar ratio used in the hydrolysis was approximately 1:1:3:7:0.1. The reactant mixtures were refluxed at 80 °C for 24 h under mechanical stirring to produce completely hydrolyzed and very stable and clear organic/Silica hybrids sol with 1:1 GPTS/TEOS ratio.

In the following step, GPTS/TEOS-derived organic/Silica sols were doped with 5 ml of Rhodamine B (used as received from Sigma–Aldrich) ethanolic solution, added to 20 ml of GPTS/TEOS-derived sol. The concentration of Rhodamine B was varied to study the fluorescence dependence and dimers formation. In this work, we use the following dye concentrations: 0.01, 0.025, 0.05, 0.1, 0.25, 0.5, 1.0, 1.25, 1.7, 2.5, and 5.0 mmol/L. Studies have shown that ionic dyes tend to aggregate in highly doped solutions, leading to dimer formation, and sometimes even higher order aggregates [35].

The GPTS/TEOS-derived organic/silica monolithic xerogels doped with Rhodamine B were prepared by adding 0.5 ml of doped sols to sealed flasks that were left 30 days at 40 °C for condensation, densification and very slow drying of the sols. After this period very dense and clear monolithic xerogels with 10 mm-diameter and 3 mm-thick were obtained. The vessel was broken and the monolithic solid material was cut in pieces of $10 \times 3 \times 2\ mm^3$ and polished using a wax base for polishing. UV–VIS–NIR optical absorption and fluorescence spectra were collected using a Varian Cary 50 and a Varian Cary Eclipse spectrophotometer, respectively. The measurements were carried out at room temperature.

For the waveguides fabrication, the obtained samples were micromachined using an extended-cavity Ti:sapphire laser oscillator, with a repetition rate of 5.2 MHz and a ~18-nm (FWHM) spectral bandwidth centered at 800 nm, that produces up to 100 nJ energy pulses with 50 fs of duration. The pulses were tightly focused through a (40×, 0.67-NA) microscope objective into the sample, which was translated at a constant speed with respect to the laser beam. The schematic setup can be seen in Fig. 1(a). The fs-laser beam was focused into the 2-mm-thick sample, approximately 120 μm below its surface. Waveguides were written along the entire 3-mm length of the sample, and spaced by 200 μm to prevent crosstalk between them. Different pulse energies and scanning speeds were investigated in the fs-laser micromachining. We evaluate pulse energies ranging 5–12 nJ and scanning speeds between 25 to 100 μm/s (25 μm/s increment). After fabrication, the geometrical aspects of the waveguides were observed by optical microscopy. To couple light in the fabricated waveguides, we polished the input and output faces of the sample. The final length of the waveguides was 2 mm. Fig. 1(b) shows an illustration of the experimental setup for coupling light in the waveguide. Before reaching the first microscope lens (40×, 0.67-NA), the HeNe (632.8 nm) laser beam was expanded by a telescope. The light transmitted through the waveguide is collected by a 10× microscope objective (0.25-NA) at the exit. Besides, an iris was used to block any scattered light at the exit of the second objective lens. The exit of the waveguide was imaged on a CCD camera to analyze the guided mode. In order to determine the total loss of the fabricated waveguides, we measured the laser beam power before and after the coupling system (Fig. 1(b)), taking into account all transmission factors of the system.

3. Results and discussion

The UV–VIS–NIR optical absorption spectrum of the Rhodamine B-doped GPTS/TEOS-derived monolithic xerogel (0.5 mmol/L) is shown in the black line of Fig. 2(a). As it can be seen, there is no absorption around 800 nm, wavelength used for the waveguide fabrication with fs-pulses. Also at 632.8 nm, wavelength in which the produced waveguides were tested, the sample absorbance is negligible. The normalized fluorescence spectrum of the sample is presented in Fig. 2(a) (gray line – right axis), obtained with excitation at 430 nm.

Fig. 2(a) shows the fluorescence intensity as a function of wavelength for the different Rhodamine B concentrations used in this work. Increasing the dye concentration on the sample, a red shift is observed in the maximum fluorescence wavelength [21,27]. This occurs because the fluorescence from the excited state dye molecule is reabsorbed by the ground state molecule which shifts the fluorescence peak to lower energies [36–38]. For the smallest dye concentrations used, 0.01 mmol/L, the maximum fluorescence wavelength is observed at 579 nm. The intensity of the fluorescence spectrum increases and it shifts to 600 nm at a concentration of 0.5 mmol/L, where it reaches its maximum fluorescence emission. The band tuning ranges from 579 nm to 624 nm (total red shift of 45 nm) over the concentration interval investigated. The

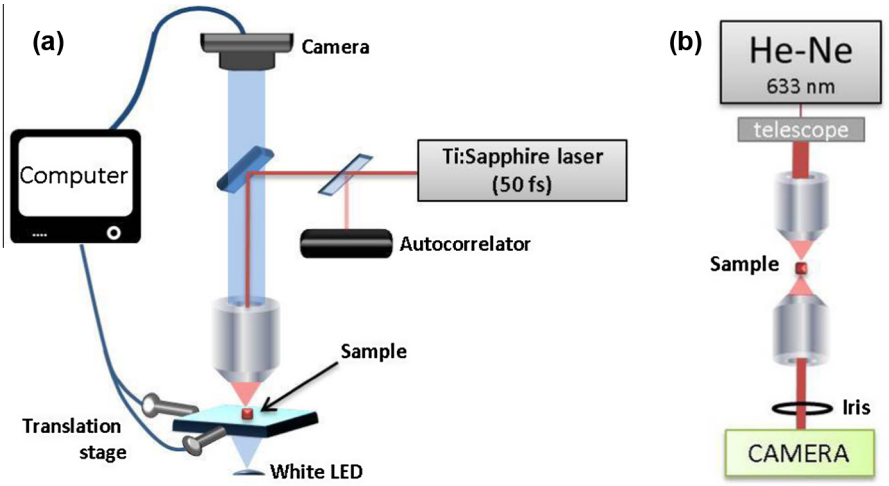

Fig. 1. Micromachining (a) and waveguide coupling (b) systems.

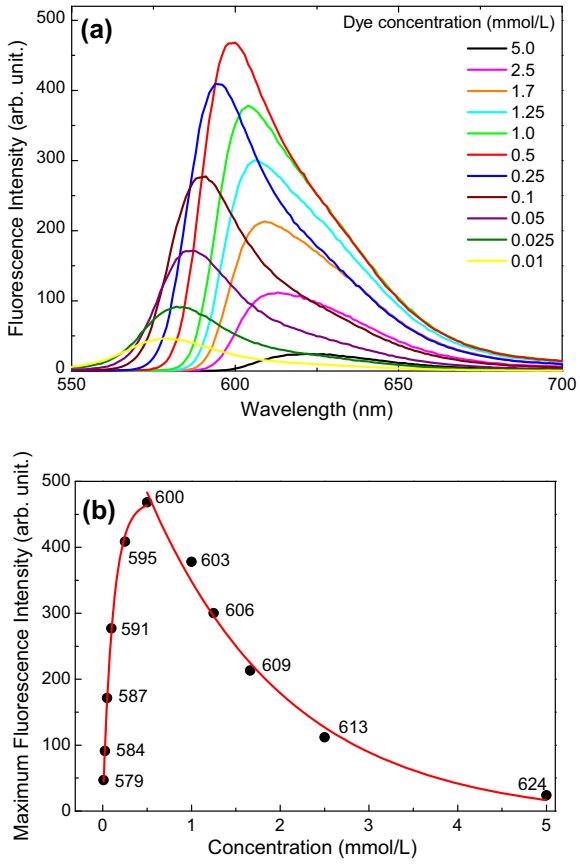

Fig. 2. (a) Fluorescence intensity for 430 nm wavelength excitation, in function of the different concentrations of Rhodamine B in the organic/silica sol. (b) Maximum fluorescence intensity, for 430 nm wavelength excitation, in function of the dye concentration in the organic/silica sol. Solid red line are monoexponential fittings of the experimental data (solid circles). Numbers represent the wavelength (nm) of the maximum fluorescence. (For interpretation of the references to color in this figure legend, the reader is referred to the web version of this article.)

maximum fluorescence intensity (solid circles) and its peak wavelength (values along the symbols) are clearly exponentially dependent on the concentration of the dye in the organic/silica sol, as shown in Fig. 2(b).

As mentioned, if the Rhodamine B concentration is increased from 0.01 mmol/L to 0.5 mmol/L, the maximum fluorescence intensity rapidly increases, reaching a maximum value for 0.5 mmol/L. In the sequence, for a dye concentration ranging from 0.5 mmol/L to 5.0 mmol/L, there is a slower exponential decrease in the maximum fluorescence intensity (Fig. 2(b)). Such reduction in the fluorescence intensity is associated with non radiative energy transfer resulting from the formation of aggregates, when the average distance among molecules is decreased [39], as well as to the relaxation between vibronic levels of Rhodamine B [40,41].

Waveguides were fabricated in Rhodamine B-doped GPTS/TEOS-derived monolithic xerogel samples with highest fluorescent intensity (0.5 mmol/L of Rhodamine B). The UV–VIS–NIR optical absorption spectrum of the doped xerogel with 0.5 mmol/L of Rhodamine B is shown in Fig. 3 (black line – right axis). The normalized fluorescence spectrum of the sample is presented in Fig. 3 (gray line – right axis), obtained with excitation at 430 nm.

Fig. 4(a) shows the top view microscopy image of a typical waveguide, fabricated with 9.6 nJ and 100 μm/s. As can be observed by the transverse view of the waveguide, displayed in Fig. 4(b), an elongated region, with a width of about 3.5 μm and

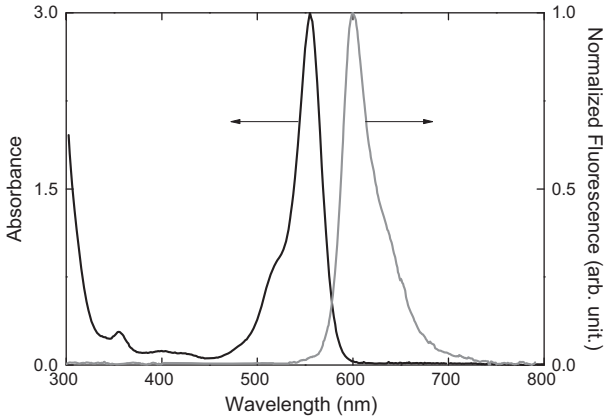

Fig. 3. Optical absorption (black line) and normalized fluorescence spectrum (gray line) of Rhodamine B-doped GPTS/TEOS xerogel sample (dye concentration of 0.5 mmol/L).

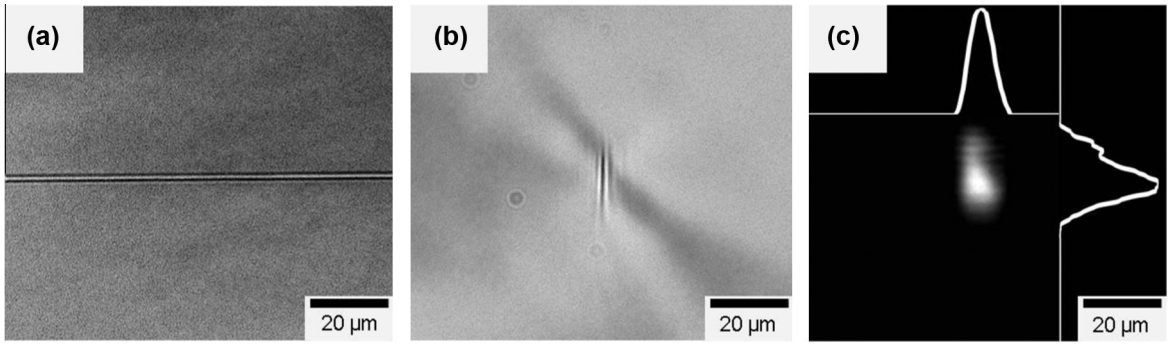

Fig. 4. (a) Optical microscopy image of waveguide produced on the bulk of the sample using pulse energy of 9.6 nJ and scanning speed of 100 μm/s. (b) A transverse image of the typical waveguide. (c) Near-field intensity distribution measured at the output of the waveguide – white lines represent horizontal and vertical intensity profiles.

height of 18 μm can clearly be observed. No micromachining has been observed for pulse energies below ~6 nJ. For pulse energies above 11.6 nJ (scanning speeds of 25, 50 and 75 μm/s), cracks were observed during the micromachining, preventing the waveguides fabrication. Such small energy range in which fs-laser micromachining is achieved, which yields non-cracked waveguides, is probably related to the high sensitivity of GPTS/TEOS-derived organic/silica xerogel to temperature and stress caused when high repetition rate lasers are used. Similar results were observed for waveguides fabricated at scanning speeds of 25, 50 and 75 μm/s.

After initial alignment, non-polarized light from a HeNe laser beam (632.8 nm) was coupled into the waveguides. The near-field intensity distribution at the output of the waveguide is shown in Fig. 4(c). The horizontal mode waist obtained was 6.3 μm, which is higher than the observable waveguide width, indicating that the light is weakly confined, due to a small refractive index change produced by fs-laser writing on the waveguides [42], and the mode extends significantly outside the waveguide core. To estimate the total loss, we measured the laser beam power before and after the coupling system, taking into account all transmission factors. The produced waveguides present a total waveguide loss of (4.6 ± 0.2) dB, where the statistics were obtained by averaging 5 measurements for 3 different waveguides, with the same parameters (pulse energy of 9.6 nJ and scanning speed of 100 μm/s). Due to the sample fragility, it is not possible to discriminate the contribution from coupling and propagation. The measured absorption loss can be considered negligible.

In order to verify the possibility of self-focusing contribution in the central region of the fabricated waveguide, we also performed measurements of the nonlinear refractive index, n_2, using the traditional closed-aperture Z-scan technique [34]. As light source we have used a Ti:sapphire amplified system (CPA 2001, Clark MXR) at 775 nm with 150-fs pulses duration and operating at a 1 kHz repetition rate. To ensure a Gaussian beam TEM_{00} profile, the laser beam passes through a spatial filter before the Z-scan setup. The laser beam was focused into the sample with a 15 cm focal length lens ($w_0 = 13$ μm), and the output signal was monitored by a silicon photodetector coupled to a lock-in amplifier. We measured an undoped GPTS/TEOS sample ($L = 0.855$ mm) and, for calibration purposes, we have also measured fused silica ($L = 1.220$ mm), which has a well-known value of n_2 (2.4×10^{-16} cm^2/W) [43], using a laser irradiance of 1.7×10^{11} W/cm^2. The Z-scan curves are shown in Fig. 5. We obtained the undoped GPTS/TEOS refractive nonlinearity ($n_2 = 4.8 \times 10^{-16}$ cm^2/W) is twice of that of fused silica, indicating that the positive n_2 can affect the light intensity profile and, consequently, the shape of the central portion of the fabricated waveguide due to self-focusing [44,45].

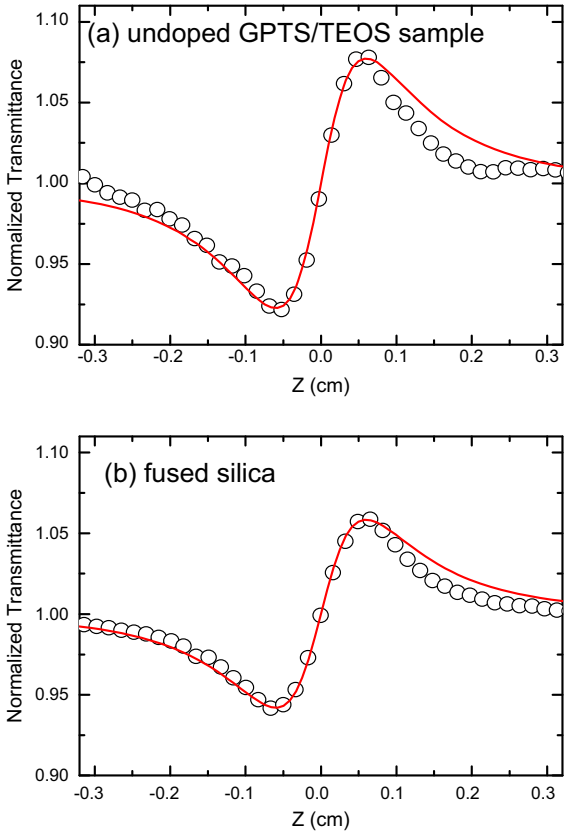

Fig. 5. Experimental closed-aperture Z-scan curves at 775 nm (open circles). The n_2 obtained for the undoped GPTS/TEOS bulk sample (a) is two times higher than fused silica (a). The solid line represents the fitting employing the theory described in Ref. [34].

4. Conclusion

In summary, we have presented results of the fabrication of waveguides inside Rhodamine B doped GPTS/TEOS bulk material using a high energy MHz repetition rate femtosecond laser oscillator. We obtained waveguides in a small energy range between 6 and 11.6 nJ. For lower energies, there are no waveguides produced, and for higher energies, cracks were observed during the micromachining, which prevented the waveguides fabrication. The produced waveguides present a total loss of (4.6 ± 0.2) dB and the waveguide elongated profile was attributed to self-focusing effect.

Acknowledgements

Financial support from FAPESP (Fundação de Amparo à Pesquisa do Estado de São Paulo) (Processes number: 2011/12399-0, 2011/23587-1, 2011/22787-7, and 2012/04794-9), CNPq (Conselho Nacional de Desenvolvimento Científico e Tecnológico), CAPES (Coordenação de Aperfeiçoamento de Pessoal de Nível Superior) and the Air Force Office of Scientific Research (FA9550-12-1-0028) are acknowledged.

References

[1] K. Minoshima et al., Photonic device fabrication in glass by use of nonlinear materials processing with a femtosecond laser oscillator, Opt. Lett. 26 (19) (2001) 1516–1518.
[2] A.M. Streltsov, N.F. Borrelli, Fabrication and analysis of a directional coupler written in glass by nanojoule femtosecond laser pulses, Opt. Lett. 26 (1) (2001) 42–43.
[3] K. Yamada et al., In situ observation of photoinduced refractive-index changes in filaments formed in glasses by femtosecond laser pulses, Opt. Lett. 26 (1) (2001) 19–21.
[4] M. Will et al., Optical properties of waveguides fabricated in fused silica by femtosecond laser pulses, Appl. Opt. 41 (21) (2002) 4360–4364.
[5] W. Watanabe et al., Wavelength division with three-dimensional couplers fabricated by filamentation of femtosecond laser pulses, Opt. Lett. 28 (24) (2003) 2491–2493.
[6] T. Shih et al., Faraday rotation in femtosecond laser micromachined waveguides, Opt. Express 15 (9) (2007) 5809–5814.
[7] Y. Nasu, M. Kohtoku, Y. Hibino, Low-loss waveguides written with a femtosecond laser for flexible interconnection in a planar light-wave circuit, Opt. Lett. 30 (7) (2005) 723–725.
[8] A.M. Kowalevicz et al., Three-dimensional photonic devices fabricated in glass by use of a femtosecond laser oscillator, Opt. Lett. 30 (9) (2005) 1060–1062.
[9] L. Eldada, L.W. Shacklette, Advances in polymer integrated optics. Selected topics in quantum electronics, IEEE J. 6 (1) (2000) 54–68.
[10] K.M. Davis et al., Writing waveguides in glass with a femtosecond laser, Opt. Lett. 21 (21) (1996) 1729–1731.
[11] B.H. Cumpston et al., Two-photon polymerization initiators for three-dimensional optical data storage and microfabrication, Nature 398 (6722) (1999) 51–54.
[12] S. Maruo, O. Nakamura, S. Kawata, Three-dimensional microfabrication with two-photon-absorbed photopolymerization, Opt. Lett. 22 (2) (1997) 132–134.
[13] D.S. Correa et al., Femtosecond laser in polymeric materials: microfabrication of doped structures and micromachining. Selected topics in quantum electronics, IEEE J. 18 (1) (2012) 176–186.
[14] Y. Shimotsuma et al., Nanofabrication in transparent materials with a femtosecond pulse laser, J. Non-Cryst. Solids 352 (6–7) (2006) 646–656.
[15] T.Q. Jia et al., Formation of nanogratings on the surface of a ZnSe crystal irradiated by femtosecond laser pulses, Phys. Rev. B 72 (12) (2005) 4.
[16] T.-S. Deng et al., One-step synthesis of highly monodisperse hybrid silica spheres in aqueous solution, J. Colloid Interface Sci. 329 (2) (2009) 292–299.
[17] D. Zhao et al., Nonionic triblock and star diblock copolymer and oligomeric surfactant syntheses of highly ordered, hydrothermally stable, mesoporous silica structures, J. Am. Chem. Soc. 120 (24) (1998) 6024–6036.
[18] U. Posset et al., Structure–property correlations in hybrid sol–gel coatings as revealed by Raman spectroscopy, Opt. Mater. 26 (2) (2004) 173–179.
[19] R.W. Jones, Fundamental Principles of Sol–Gel Technology, The Institute of Metals, London, 1990.
[20] C.J.S. Brinker, G.W., Sol–Gel Science. The Physics and Chemistry of Sol–Gel Processing, first ed., Academic Press, 1990, p. 912.
[21] F. del Monte, J.D. Mackenzie, D. Levy, Rhodamine fluorescent dimers adsorbed on the porous surface of silica gels, Langmuir 16 (19) (2000) 7377–7382.
[22] M. Keränen et al., Synthesis and characterization of optical sol–gel adhesive for military protective polycarbonate resin, J. Sol–Gel Sci. Technol. 31 (1–3) (2004) 369–372.
[23] M.A. Robertson et al., Mechanical and thermal properties of organic/inorganic hybrid coatings, J. Sol–Gel Sci. Technol. 26 (1–3) (2003) 291–295.
[24] Y.-L. Liu, Y.-H. Su, J.-Y. Lai, In situ crosslinking of chitosan and formation of chitosan–silica hybrid membranes with using γ-glycidoxypropyltrimethoxysilane as a crosslinking agent, Polymer 45 (20) (2004) 6831–6837.
[25] F. Peng et al., Hybrid organic–inorganic membrane: solving the tradeoff between permeability and selectivity, Chem. Mater. 17 (26) (2005) 6790–6796.
[26] C. Sanchez et al., Designed hybrid organic–inorganic nanocomposites from functional nanobuilding blocks, Chem. Mater. 13 (10) (2001) 3061–3083.
[27] C.M. Carbonaro et al., On the formation of aggregates in silica–rhodamine 6G type II hybrids, RSC Adv. 2 (5) (2012) 1905–1912.
[28] F. Liu, B. Sanyasi Rao, J.-M. Nunzi, A dye functionalized silver–silica core–shell nanoparticle organic light emitting diode, Org. Electron. 12 (7) (2011) 1279–1284.
[29] W. Arap et al., Luminescent silica nanoparticles for cancer diagnosis, Curr. Med. Chem. 20 (17) (2013) 2195–2211.
[30] A. Auger et al., A comparative study of non-covalent encapsulation methods for organic dyes into silica nanoparticles, Nanoscale Res. Lett. 6 (2011) 12.
[31] L.D.S. Alencar et al., High fluorescence quantum efficiency of CdSe/ZnS quantum dots embedded in GPTS/TEOS-derived organic/silica hybrid colloids, Chem. Phys. Lett. 599 (2014) 63–67.
[32] Y. Yang et al., The influence of oscillator configurations on performance of solid-state dye laser medium prepared by a new mould fabrication technique, Mater. Lett. 57 (3) (2002) 660–665.
[33] A. Parvathy Rao, A. Venkateswara Rao, Luminiscent dye Rhodamine 6G doped monolithic and transparent TEOS silica xerogels and spectral properties, Sci. Technol. Adv. Mater. 4 (2) (2003) 121–129.
[34] M. Sheik-bahae, A.A. Said, E.W. Van Stryland, High-sensitivity, single-beam n2 measurements, Opt. Lett. 14 (17) (1989) 955–957.
[35] L., et al., UV–Vis spectroscopic and chemometric study on the aggregation of ionic dyes in water, Talanta 49(1) (1999) 99–106.
[36] F.L. Arbeloa, P.R. Ojeda, I.L. Arbeloa, Fluorescence self-quenching of the molecular-forms of Rhodamine-B in aqueous and ethanolic solutions, J. Lumin. 44 (1–2) (1989) 105–112.
[37] F.L. Arbeloa, P.R. Ojeda, I.L. Arbeloa, On the aggregation of Rhodamine-B in ethanol, Chem. Phys. Lett. 148 (2–3) (1988) 253–258.
[38] A. Kurian et al., Studies on fluorescence efficiency and photodegradation of rhodamine 6G doped PMMA using a dual beam thermal lens technique, Laser Chem. 20 (2–4) (2002) 99–110.
[39] F. del Monte, D. Levy, Identification of oblique and coplanar inclined fluorescent J-dimers in Rhodamine 110 doped sol–gel-glasses, J. Phys. Chem. B 103 (38) (1999) 8080–8086.
[40] M. Fikry, M.M. Omar, L. Ismail, Effect of host medium on the fluorescence emission intensity of Rhodamine B in liquid and solid phase, J. Fluoresc. 19 (4) (2009) 741–746.
[41] T.H. Nhung et al., Dye energy transfer in xerogel matrices and application to solid-state dye lasers, Opt. Commun. 232 (1–6) (2004) 343–351.
[42] V.R. Bhardwaj et al., Femtosecond laser-induced refractive index modification in multicomponent glasses, J. Appl. Phys. 97 (8) (2005).
[43] D. Milam, Review and assessment of measured values of the nonlinear refractive-index coefficient of fused silica, Appl. Opt. 37 (3) (1998) 546–550.
[44] A. Saliminia et al., Writing optical waveguides in fused silica using 1 kHz femtosecond infrared pulses, J. Appl. Phys. 93 (7) (2003) 3724–3728.
[45] M. Ams et al., Slit beam shaping method for femtosecond laser direct-write fabrication of symmetric waveguides in bulk glasses, Opt. Express 13 (15) (2005) 5676–5681.